

## Investigation of Facial Region of Interest in Infrared Images for Real-Time Noncontact Respiration Monitoring

Abdulkadir Hamidu Alkali\*, Reza Saatchi\*, Heather Elphick\*\*, Derek Burke\*\*

\* Faculty of ACES, Sheffield Hallam University, Sheffield, UK, [a.alkali@shu.ac.uk](mailto:a.alkali@shu.ac.uk), [r.saatchi@shu.ac.uk](mailto:r.saatchi@shu.ac.uk)

\*\*Sheffield Children's Hospital, NHS Trust, Sheffield, UK, [heather.elphick@sch.nhs.uk](mailto:heather.elphick@sch.nhs.uk), [derek.burke@sch.nhs.uk](mailto:derek.burke@sch.nhs.uk)

### Abstract

In this study thermal imaging was used to monitor respiration rate in a noncontact manner. The main focus was to investigate the shape of a region under the nose (called the region of interest, ROI) and the characterisation of this region by a representative feature to produce a respiration signal from which respiration rate was obtained. It was demonstrated that the respiration signal from a rectangular ROI produces least respiration signal drift as compared with circular and elliptic shapes. The circular ROI provided a larger magnitude respiration signal and the mode of the pixel values contained in it provided the best statistical measure for determining respiration rate as compared with median, standard deviation and mean. Rectangular ROI had a faster response to the changes in RR as compared with the other statistical measures used to represent the ROI.

### 1. Introduction

The human body requires oxygen, which is found in air, for all its metabolic activities. Carbon dioxide is produced as a waste after the metabolic activity and has to be transported from the body. The body therefore requires a constant supply of air containing oxygen and the removal from the lungs of oxygen consumed air. This process is achieved by respiration mechanisms. Respiration starts with inspiration when the diaphragm and the intercostal muscles contract to make the rib cage to move upwards resulting in an increased volume of the thoracic cavity that expands the lungs. This process makes the air pressure within the lungs to be lower than that of the atmosphere and thus obeying the Boyle's law, air moves from the atmosphere into the lungs through the trachea [1]. Expiration completes a respiration cycle when the air expires from the lungs as a result of the elastic nature of the thoracic wall that forces the rib cage to move down and inwards. The processes of inspiration and expiration completes one respiration cycle.

Average respiration rate in cycles per minute (cpm) is known as respiratory rate (RR). RR varies depending on the subject's physical activity, gender, age as well as subject's wellbeing [2]. In healthy adults RR is between 12 - 20 cpm [3], but is significantly higher in children and infants. Methods to monitor respiratory rate can be classified as contact and non-contact [4]. In the former, a device is attached to the subject's body, while in the later physical contact is not required. In both types, the monitoring is performed through utilisation of an effect that is produced as a result of respiration [5]. The most common effects are changes in abdomen and chest position, changes in the temperature of expired and inspired air, changes in expired air flow and variations in infrared emission from the skin surface centred on the nose and mouth. These were utilised in different studies to measure respiration rate [2, 5-12].

Contact approaches suffer from a number of shortcomings, e.g. subject discomfort caused by the attached sensing device that leads to inaccuracies in the respiration rate, failure of the recording when sensor is dislodged and complexity in attaching the device to the body. There are also concerns associated with safety issues when an electrical device is attached to the body.

Studies have shown that respiratory rate is an important indicator of a person's wellbeing and is a better discriminator between stable and unstable patients [4, 13, 14]. This important vital sign is mostly not monitored as observed by Cretikos et al [15]. Lack of extensive RR monitoring may be as a result of the complexities associated with the contact devices. To encourage monitoring of RR as well as improve its accuracy, a device that monitors respiration in a noncontact manner will play a significant role

In this study thermal imaging was used to monitor RR in a noncontact manner. As air expire from the nose a region around the rip of the nose, especially under the nostril become warmer, emitting an increased amount of infrared radiation. As air is inhaled the effect is reversed. The approached required identification of the relevant area on the face that provides best indication of infrared variations produced by respiration (i.e. the respiration region of interest, ROI), tracking this region in successive images, even with head and body movements, representing the region that contains pixel values of temperature by a suitable feature, producing a respiration signal from the extracted feature across a series of images recorded over time, and finally obtained RR value from the signal. The focus on this study is on the shape and size of the ROI and comparison of a number of features to best represent it.

In the following sections, the methodology used to obtain results is explained, the results are discussed and the main conclusions are provided.

## 2. Methodology

A FLIR A40 thermal camera with the specifications indicated in Table 1 was used for the study.

**Table 1: Specification of the thermal camera**

Camera Parameter	Specification
Spectral range	7.5 $\mu\text{m}$ to 13.0 $\mu\text{m}$
Thermal sensitivity	0.08 Kelvin
Image size	320 by 240 pixels
Image sequence	16-bit monochrome

In order to perform the investigation, respiration was monitored on an adult subject for about three minutes. The image filtering, segmentation and tracking (of ROI) methods used in the study were reported in our earlier study [2]. Briefly, the procedure required high-pass filtering of the first captured image and pre-selecting a template centred on the tip of the nose. The template was stored as a reference for identifying the selected region in the subsequent images. A point of interest (POI) was then selected beneath the nose skin surface as this region is affected by respiration by other regions of the face. These selections were performed once at the start of recording.

Each image recorded was high-pass filtered and then the subject was segmented from the image background. The subject's face was then identified and enclosed in a rectangle to indicate detection. The template was then searched for within the detected (enclosed) face and the POI was also updated since the pixel distance between the template and the point of interest remained constant. This updating was required as the respiration POI appeared in different locations in the recorded images due to head movements. A region of interest (ROI) was then created at the POI and the infrared emitted within it were extracted and processed as a respiration feature. The reason for first selecting a template and then using it to identify the POI, is that the template temperature characteristics as a whole would remain consistent during the recording. The template could not be chosen under the nose as the temperature in this area changes due to respiration and thus cannot be used directly for the tracking purpose.

This process outlined above was repeated for each acquired image to obtain a feature of the selected ROI and then the respiration signal. The signal was filtered using a 4<sup>th</sup> order low-pass Butterworth filter with a cut-off frequency of 2 Hz. The discrete Fourier transform of the filtered signal was then obtained after windowing the signal with the Hanning window. The frequency corresponding to the highest magnitude in the frequency spectrum was then identified and multiplied by 60 to obtain RR in cycle per minute (CPM).

The contribution of this study is determining the best shape, size of the ROI and comparing possible features that could be used to characterise the region. Instead of using rectangular ROI (as in previous studies) and then averaging (i.e. mean statistical feature) the temperature values with this rectangle, three different shapes for ROI were investigated in addition to the using the mean, a number of other statistical features were investigated. The shapes investigated for the ROIs were circle, rectangle and ellipse with areas and dimensions as indicated in Table 2. The statistical features were the mean, median, mode, standard deviation, root-mean-square (RMS) value and variance.

**Table 2: Dimensions of the various ROIs**

Dimensions		Circle	Rectangle	Ellipse
		Diameter = 15	Length, Width = 11,16	a,b = 11,5
Area (pixels <sup>2</sup> )	Calculated	176.71	176	172.79
	Measured	177	176	172

Each ROI was created on the updated location of point of interest (POI) and overlaid to indicate location and shape. The infrared emitted within the ROIs were extracted by considering the pixel values within the ROI. The three shapes for the ROI that were used are mostly used in studies involving use of ROIs. The extracted array had equal columns for all rows but only the pixels within the ROI had values greater than one while the rest were padded with zeros. To get the actual number of pixels in a ROI, the total number of pixels in an array for the ROI that had a value greater than one was counted. This was so that padded pixels (zeros) were not taken as valid pixels. The variations in the number of pixels obtained by calculation and measurement are as a result of some pixels being located on the POI boundary.

A number of algorithms were developed to extract the specified ROIs according to the shape required. For an ellipse, all pixels at coordinates that satisfied the general equation of an ellipse (equation 1) were extracted.

$$\frac{(\bar{x}-X)^2}{a^2} + \frac{(\bar{y}-Y)^2}{b^2} \leq 1 \quad (1)$$

Where  $\check{x}$  and  $\check{y}$  are the x and y axis coordinates of a pixel in reference, X and Y are the x and y coordinates of the POI, a and b are the radius along the x and y axis respectively. The same equation was used for a circle but with:

$$a = b = r = \frac{d}{2} \tag{2}$$

Where  $r$  and  $d$  are the radius diameter respectively.

The processing time for each frame was 40 milliseconds, allowing real-time measurement. The recording lasted for at least 3 minutes.

Once the respiration region was specified by either a circle, ellipse or rectangle, the chosen statistical measure then characterised the region and by performing the operation on the recorded images a respiration signal was produced. The signal was low pass filtered using 4<sup>th</sup> order Butterworth filter with a cut-off frequency of 2 Hz and then first 512 features of the signal was windowed using a Hanning window. The discrete Fourier transform (DFT) of the windowed signal was obtained. The frequency associated with the largest peak in the magnitude frequency spectrum was identified and its value was multiplied by 60 to produce RR in CPM (cycles per minute). To obtain the RR over time, 512 features were first considered. Thereafter, the feature was moved by four signal points by considering 4 new features in addition to the previous 508 features and then obtaining the RR. The obtained RR was for the oldest feature on the signal. The RR was then plotted over time as it was made available and was also used in comparing the effect of the ROIs as well as the statistical measures on RR. The statistical methods were used in each of the three ROIs in obtaining the respiration feature and thereafter the RR.

### 3. Results and Discussions

Figure 1 show the identified ROI represented by circle, rectangle and ellipse during the recording.



**Figure 1.** From left to right, circular, rectangular and Elliptic ROIs.

The areas covered by the three ROIs were not exactly the same due to the shape of each ROI. The circle has 177 square pixels as against 176 and 172 by rectangle and ellipse respectively. The mean area was 175 square pixels with a standard deviation of 2.16. The difference is negligible to cause a significant error in comparison of the shapes.

Table 3 indicates the average amplitude of the respiration signal obtained using each of the six statistical measures for the three ROI shapes. The rectangular ROI had the largest average values when the median, standard deviation, moment and modal statistical values were considered. The circular ROI had highest average value when mean and RMS values were considered. Higher average values were a result of larger range of a signal that will provide an improved signal to noise ratio (thus making it easier to detect the signal).

**Table 3** Average signal values of the ROIs obtained using the statistical measures

Statistical measure	Average across recorded images		
	Circle	Rectangle	Ellipse
<b>Median</b>	7.87	8.00	7.86
<b>Mean</b>	7.90	7.89	7.88
<b>Standard Deviation</b>	7.91	7.94	7.93
<b>Root Mean Square</b>	7.90	7.90	7.88
<b>Moment</b>	7.92	7.95	7.94
<b>Mode</b>	8.00	8.02	7.90

Figure 2 shows plots of respiration signals obtained using the three shapes and for the statistical measures that represented (i.e. median, mean, standard deviation, root mean square, moment and mode) each shape. The standard deviation for the rectangular ROI was the least indicative of respiration signal. This indicates that variation of the signal from the mean was the least as also indicated by the non-drift nature of the RR signal as compared to that obtained

using the circular and ellipse ROIs. The rectangular ROI had the smallest fluctuation (drift) over time. The circular and elliptic ROI had signals with similar amplitudes for most statistical measures, perhaps due to shape resemblance of the two ROIs. In a whole, the signals obtained from the circular ROI had the largest amplitude and will therefore give better graphical representation of the RR over time.

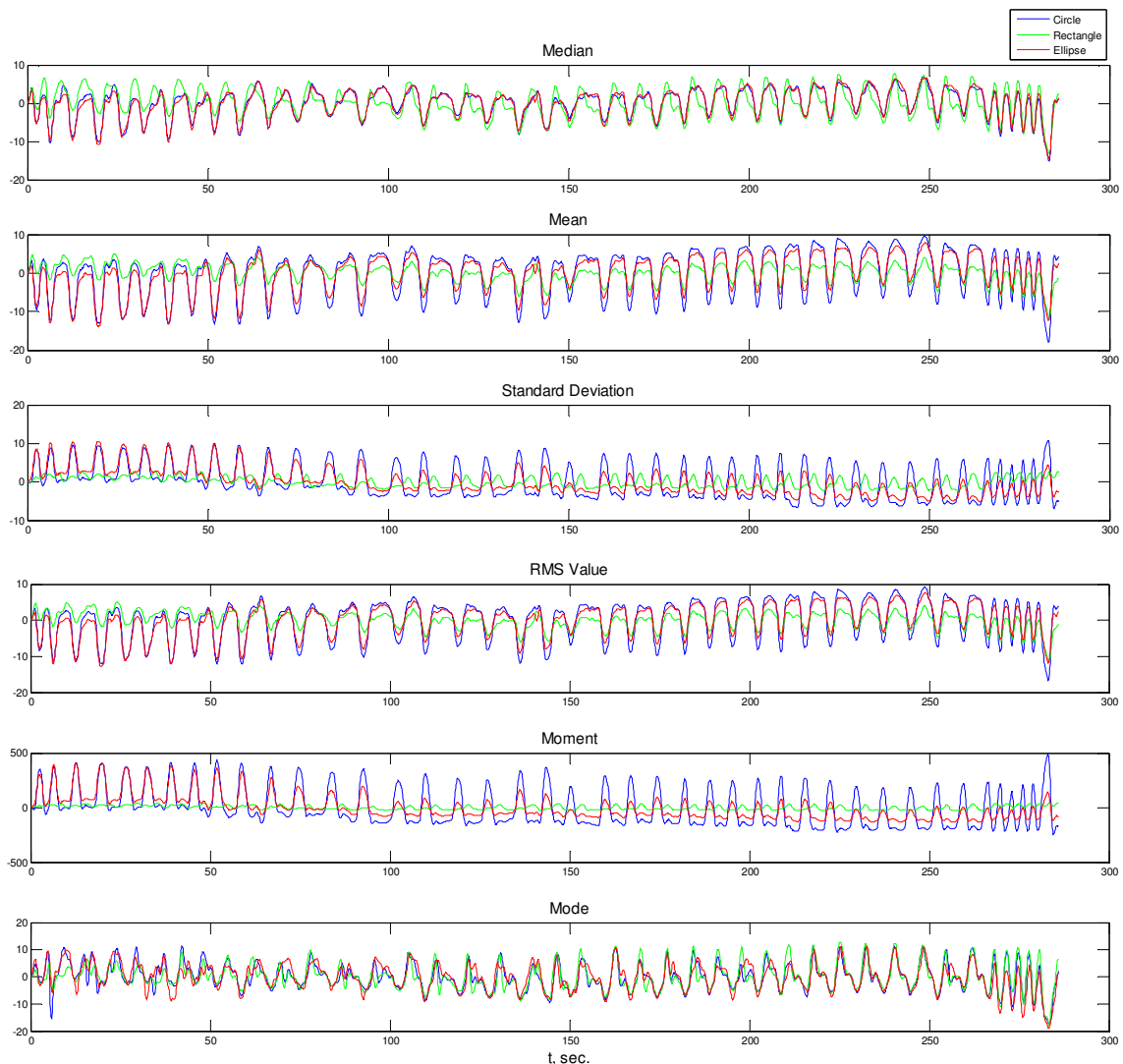


**Figure 2.** Comparing the respiration signal obtained using the various statistical measures in the three ROIs

For the circular ROI, the RR obtained using the mode was best representative of a respiration signal as it had the highest signal average value. For the elliptic ROI, the mode gave best respiration signal. Mode also gave best respiration signal for the rectangular ROI. There were drifts in the signals obtained using the circle and ellipse ROIs while that obtained using the rectangular ROI almost had no drift.

Figure 3 shows the RR over time obtained using the three ROIs and the statistical measures. For the circular ROI, the mode responded to the variations in RR faster while the mean was slightly responsive during the beginning and towards the end of monitoring. The mode was also most responsive to small variations in RR derived from the elliptic ROI. The mode lagged behind the other measures in updating the changes in RR. This can be seen around the 140<sup>th</sup> and 205<sup>th</sup> seconds of the circular and ellipse ROIs derived RR as well as around the 60<sup>th</sup> second on the ellipse derived ROI RR. The mode was also earlier in registering RR changes that are indicated around the 170<sup>th</sup> second on the circular derived ROI and the 70<sup>th</sup> seconds the rectangular ROI derived RR.

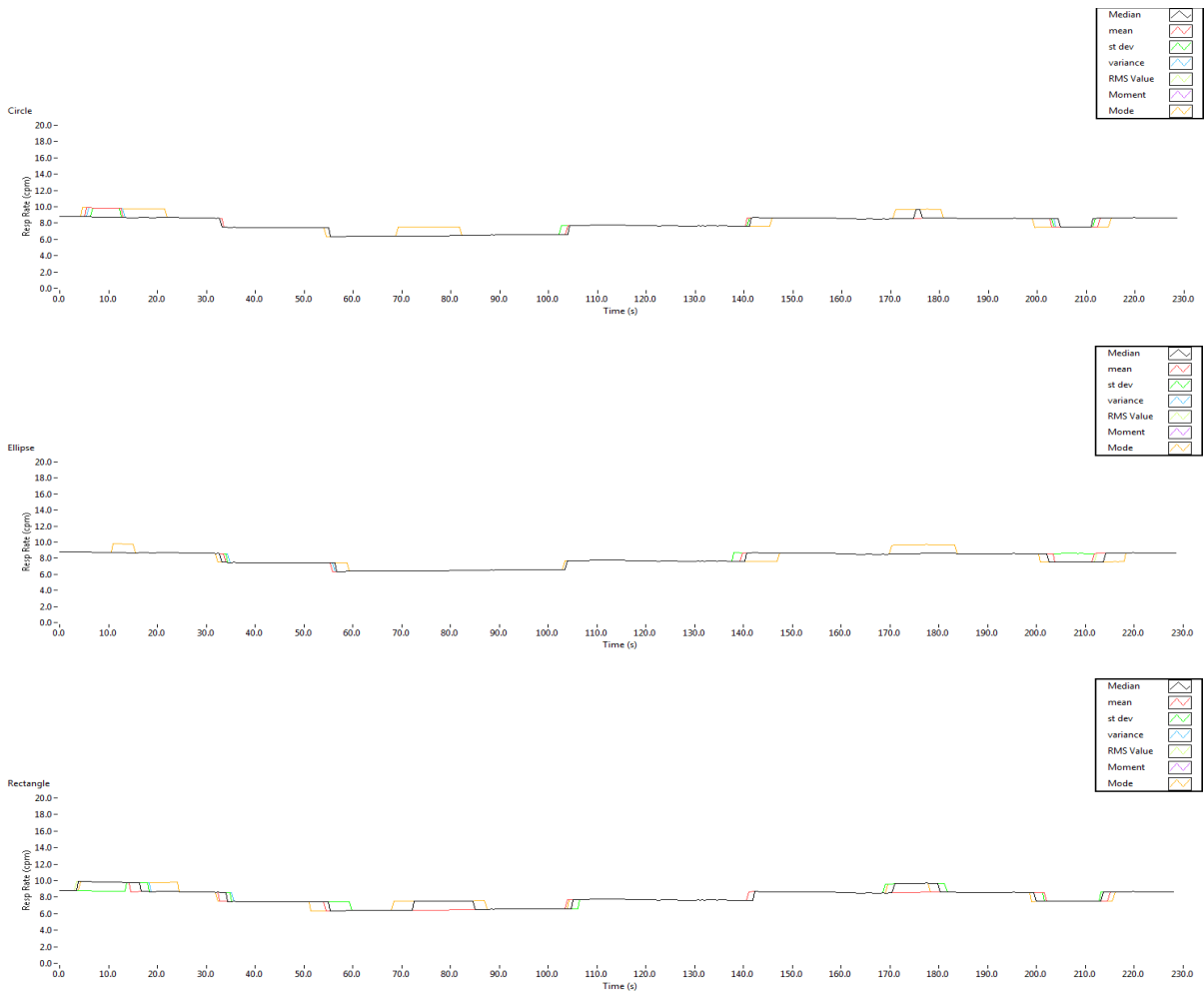


**Figure 3:** RR obtained by considering the signals from the various statistical measures using (top) circle, (middle) elliptic and (bottom) rectangular ROIs.

The performance of the mean was the worst in the rectangular ROI derived RR as it was the only one that did not register RR changes between 70 - 90 and 170 - 180 seconds.

#### 4. Acknowledgement

Abdulkadir Alkali would like to acknowledge the Petroleum Technology Development Fund (PTDF), Nigeria for his sponsorship.

#### 5. Conclusions

Six statistical measures (median, mean, standard deviation, root mean square, moment and mode) were used to obtain the respiration signal feature from three respiration region of interest derived from three shapes; circle, rectangle and ellipse. The amplitude of the respiration signal and respiration rates were considered in the comparisons. It was found that the respiration signal derived from rectangle ROI irrespective of the statistical measure used had the least drift. The respiration signal derived from the circular ROI in all six statistical measures gave the largest amplitude. The mode gave the best characterisation of respiration rate over time in the three ROIs considered, while the rectangular ROI had a better response to changes in RR when all the statistical measures were considered as compared to the circular and elliptic ROIs for the same purpose.

## REFERENCES

- [1] Mader S. S., "Maintenance of the human body," in Human Biology, 9th ed. Anonymous 2006, pp. 141-158.
- [2] Alkali A. H., Saatchi R., Elphick H. and Burke D., "Facial tracking in thermal images for real-time noncontact respiration rate monitoring," in Modelling Symposium (EMS), 2013 European, 2013, pp. 265-270.
- [3] Parkes R., "Rate of Respiration: the Forgotten Vital Sign," *Emerg. Nurse*, vol. 19, pp. 12-18, 2011.
- [4] AL-Khalidi F. Q., Saatchi R., Burke D., Elphick H. and Tan S., "Respiration rate monitoring methods: A review," *Pediatr. Pulmonol.*, vol. 46, pp. 523-529, 2011.
- [5] Alkali A. H., Saatchi R., Elphick H., Burke D. and Evans R., Noncontact respiration rate monitoring based on sensing exhaled air. *Malaysian Journal of Fundamental and Applied Sciences (MJFAS)*, vol. 9, no.3, pp. 129. 2013.
- [6] AL-Khalidi F. Q., Saatchi R., Burke D. and Elphick H., "Facial tracking method for noncontact respiration rate monitoring," in Communication Systems Networks and Digital Signal Processing (CSNDSP), 2010 7th International Symposium on, 2010, pp. 751-754.
- [7] Aoki H., Miyazaki M., Nakamura H., Furukawa R., Sagawa R. and Kawasaki H., "Non-contact respiration measurement using structured light 3-D sensor," in SICE Annual Conference (SICE), 2012 Proceedings of, 2012, pp. 614-618.
- [8] Corbishley P. and Rodríguez-Villegas E., "Breathing detection: Towards a miniaturized, wearable, battery-operated monitoring system," in *IEEE transaction on bio-medical engineering*, 2008, pp. 196-204.
- [9] Droitcour A. D., "Non-Contact Measurement of Heart and Respiration Rates with a Single-Chip Microwave Doppler Radar," PhD thesis, Stanford University. 2006.
- [10] Min S. D., Yoon D. J., Yoon S. W., Yun Y. H. and Lee M., "A study on a non-contacting respiration signal monitoring system using Doppler ultrasound," *Med. Biol. Eng. Comput.*, vol. 45, pp. 1113-1119, 2007.
- [11] Murthy R. and Pavlidis I., "Noncontact measurement of breathing function," *IEEE Engineering in Medicine and Biology Magazine : The Quarterly Magazine of the Engineering in Medicine & Biology Society*, vol. 25, pp. 57-67, 2006.
- [12] Tan K. S., Saatchi R., Elphick H. and Burke D., "Real-time vision based respiration monitoring system," in Communication Systems Networks and Digital Signal Processing (CSNDSP), 2010 7th International Symposium on, 2010, pp. 770-774.
- [13] Churpek M. M., Yuen T. C., Huber M. T., Park S. Y., Hall J. B. and Edelson D. P., "Predicting cardiac arrest on the wards: a nested case-control study," *Chest*, vol. 141, pp. 1170-1176, 2012.
- [14] Hammond N. E., Spooner A. J., Barnett A. G., Corley A., Brown P. and Fraser J. F., "The effect of implementing a modified early warning scoring (MEWS) system on the adequacy of vital sign documentation," *Australian Critical Care*, vol. 26, pp. 18-22, 2013.
- [15] Cretikos M. A., Bellomo R., Hillman K., Chen J., Finfer S. and Flabouris A., "Respiratory rate: the neglected vital sign," *The Medical Journal of Australia*, vol. 188, pp. 657-659, 2008.